Article

Intrinsically Atomic-Disordered LuCuTe$_2$ as a Promising Thermoelectric Material

Xiaoyu Zhang,[†] Changyuan Li,[†] Yuting Meng, Long Yang,* and Wen Li*

Cite This: https://doi.org/10.1021/acsaem.4c00763

Read Online

ACCESS | Metrics & More | Article Recommendations | SI Supporting Information

ABSTRACT: The intrinsic disorder of atoms, which facilitates additional phonon scattering and consequently reduces the lattice thermal conductivity (κ_L), serves as a guiding principle in the search for promising thermoelectric materials. This motivated us to investigate the transport properties in a new thermoelectric candidate, LuCuTe$_2$, which has intrinsically disordered cations in the structure. The atomic disordering results in a κ_L value smaller than 1.0 W/m K across the measured temperature range. The underlying material properties are revealed by the single parabolic band model, which enables a reasonable prediction of electrical transport properties for LuCuTe$_2$. The comparable transport properties along the directions perpendicular and parallel to the hot-pressing direction identify the isotropic transport behavior. Eventually, a peak thermoelectric figure of merit, zT, of ~0.8, is achieved. This work suggests that this material can be a promising thermoelectric candidate and provides guidance for further study.

KEYWORDS: thermoelectrics, LuCuTe$_2$, atomic disorder, transport properties, figure of merit
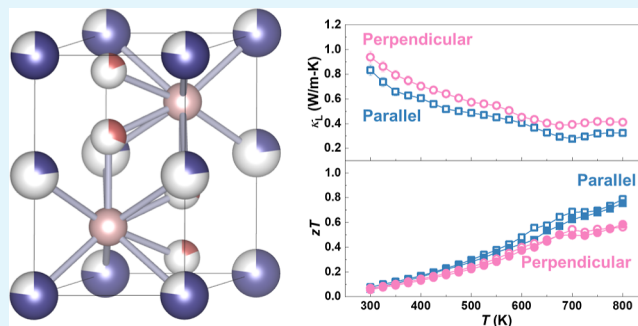
1. INTRODUCTION

Thanks to the merits of no-noise operation, no moving parts, and emission-free nature, the thermoelectric technique has emerged as a sustainable way to address the energy issue and environmental crisis. However, its relatively low conversion efficiency significantly hinders its applications on a large scale. The thermoelectric performance is described by the thermoelectric material's dimensionless figure of merit, zT, which depends on the material parameters of Seebeck coefficient S, resistivity ρ, absolute temperature T, and electrical κ_E and lattice κ_L thermal conductivity, via $zT = S^2T/\rho(\kappa_E + \kappa_L)$. Therefore, enhancing zT is identified as a critical route to advancing thermoelectric applications.

Note that a high band degeneracy (N_v),[1] low inertial effective mass (m_I^*),[2] and deformation potential coefficient (E_{def})[3] are beneficial for a superior power factor (PF = S^2/ρ).[4] Band convergence, which can be achieved through manipulating chemical constituents[5] or crystal symmetries,[6] has been proven as an effective strategy for N_v-increase and thereby significant PF-improvement. This strategy has been extensively applied to significantly enhance zT across a range of thermoelectric materials, including IV−VI compounds,[7−10] Mg$_2$Si,[5] Mg$_3$Sb$_2$,[11] half-Heusler,[12,13] Te,[14] CoSb$_3$,[15] and Zintl compounds.[16,17]

Strengthening phonon scattering to reduce κ_L is an alternative strategy to enhance zT, which can be achieved by introducing different types of defects, such as 0D point defects,[18] 1D dislocations,[19−21] and 2D nanostructures.[22,23]

Alongside the use of established band and defect strategies to enhance zT in known thermoelectric materials, exploring novel thermoelectric materials is another vital pathway for the advancement of thermoelectric applications. Materials with specific characteristics can be associated with an intrinsically low κ_L, such as a large primitive cell,[24] weak chemical bonding,[25,26] disordered atoms,[27,28] and strong lattice anharmonicity.[29,30] These crystal structure characteristics become the guiding principles in the search for novel and high-performance thermoelectric materials.

Ternary rare-earth copper-containing tellurides (ReCuTe$_2$, Re = Tb, Dy, Lu, Ho, Er, Tm), crystallizing in space $P\bar{3}m1$ group structure with partial occupation of the cations, have been demonstrated to exhibit semiconducting behavior.[31−33] The richness in composition offers the potential for the chemical manipulation of transport properties. The presence of intrinsic Cu vacancies in TmCuTe$_2$ leads to a low κ_L of ~1.0 W/m K at room temperature.[34] A zT higher than 0.8 has been frequently realized in RECuTe$_2$ (RE = Tb, Dy, Ho, Er, and Tm), suggesting these compounds as promising candidates for thermoelectric applications.

LuCuTe$_2$ shows occupation of two Lu atoms at 1a and 1b sites with a probability of 76.5 and 23.5%, respectively, while two Cu atoms occupy 2d sites by 31 and 19%.[33] Such random and/or partial occupations for both cations would significantly strengthen the material's anharmonicity, enabling strong phonon scattering for an expected lower κ_L,[35] as compared to that of ReCuTe$_2$ with a disorder of one cation. Moreover, the transport properties of LuCuTe$_2$ have rarely been studied.

Therefore, this work focuses on revealing the thermoelectric transport properties of LuCuTe$_2$. A κ_L smaller than 1.0 W/m K is achieved in this material across the measured temperature range under study. This can be attributed to the highly disordered cations, as evidenced by the Rietveld structural refinement of X-ray diffraction (XRD) data. The single parabolic band (SPB) model, incorporating acoustic scattering, provides a useful framework for understanding material parameters and making reasonable predictions about transport properties. Eventually, the sufficiently high zT of ∼0.8 at 800 K for LuCuTe$_2$ underscores its potential as a promising thermoelectric material.

2. MATERIALS AND METHODS

LuCu$_{1-x}$Cd$_x$Te$_2$ ($0 \leq x \leq 0.09$) samples were prepared by sealing the elements (>99.9%) according to stoichiometric amounts, melting at 1373 K for 10 h, and then quenching in cold water. The obtained ingots were ground into powder and further sealed in a quartz ampule for remelting at 1373 K for 10 h, annealing at 873 K for 3 d, and eventually quenching in cold water. The resulting ingots were ground into fine powders, which were sintered to form dense pellets (>96% of the theoretical density) with a diameter of ∼10 mm by the induction heating hot-press system at 700 K for 40 min under a uniaxial pressure of ∼70 MPa.

The simultaneous measurements of the Hall coefficient, resistivity, and Seebeck coefficient within 300−800 K were carried out under the protection of a helium atmosphere. Two K-type thermocouples were adhered to both sides along the pellet's radial direction to measure both the thermopower and temperature difference (ΔT). The Seebeck coefficient was derived from the slope of the thermopower versus ΔT within 0−5 K. The van der Pauw technique was utilized to measure the Hall coefficient and resistivity under a magnetic field of 1.5 T. Thermal conductivity (κ) was calculated via $\kappa = dC_pD$, where d refers to the density measured by the mass and geometric volume of the pellets and C_p represents the heat capacity estimated by the Dulong−Petit approximation with the temperature-independent assumption, and D is the thermal diffusivity obtained using the laser flash technique. There is about a 5% measurement uncertainty for these parameters.

The room-temperature optical reflectance was determined using Fourier transform infrared (FTIR) spectroscopy that is equipped with a diffuse reflectance attachment. The structural composition and microstructure were characterized by XRD and scanning electron microscopy (SEM) with an energy-dispersive spectrometer. The room-temperature sound velocity was measured by using an ultrasonic pulse receiver with an oscilloscope. Thermogravimetric analysis and differential scanning calorimetry were applied to measure the stability of the material.

The local structure was studied by using the atomic pair distribution function (PDF) technique. It gives the interatomic distance distribution beyond conventional crystallography, i.e., the probability of finding atomic pairs with distance r apart,[36] which can effectively reveal the local atomic distribution in LuCuTe$_2$. We used the rapid acquisition PDF method (RAPDF)[37] to carry out the X-ray total scattering experiments at the BL13SSW beamline at the Shanghai Synchrotron Radiation Facility. The PDF total scattering data processing and structural refinements were carried out by pyFAI, PDFgetX3, and PDFgui software packages.[38−41] The detailed PDF

experimental information can be found in the Supporting Information.

The first-principles calculation was performed with a special quasi-random structure (SQS) model[42] of LuCuTe$_2$. For the first-principles calculation, a model with a random structure represented by average atomic occupancy is often not utilized directly.[43] The SQS model generated by the Alloy Theoretic Automated Toolkit (ATAT) code[44] can usually lead to a reasonable periodic supercell approximation for the partially occupied structure of LuCuTe$_2$. This modeling approach has been widely used for disordered solid solution system calculation.[45−47] Here, a supercell model of LuCuTe$_2$ with 80 atoms and 80 vacancies was generated by ATAT for first-principles calculations. The band structure calculation was performed with the Quantum ESPRESSO 7 code[48,49] using the Perdew−Burke−Ernzerhof (PBE) exchange−correlation functional,[50] and a plane-wave basis set with a kinetic energy cutoff extended to 500 eV was taken for all calculations. The energy and force convergence criteria of calculations were set to 10^{-4} eV and 0.05 eV Å^{-1}, respectively.

3. RESULTS AND DISCUSSION

The LuCuTe$_2$ crystal structure (space group: $P\bar{3}m1$), as shown in Figure 1a, exhibits a layered structure in the sequence of A−
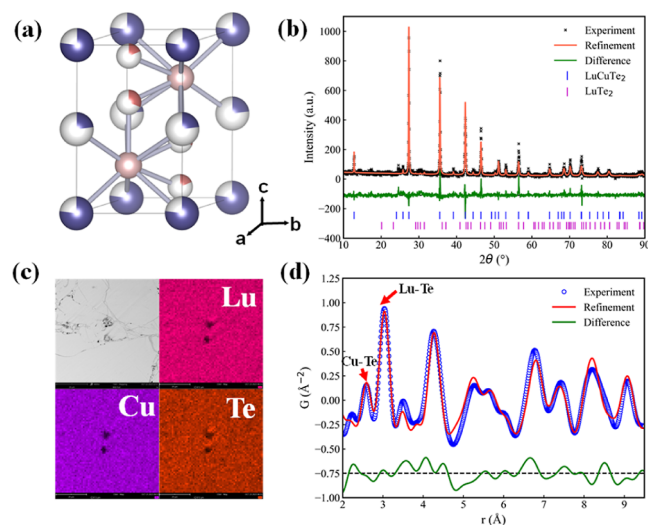

Figure 1. (a) Crystal structure of the unit cell for LuCuTe$_2$ at room temperature (Lu, Cu, and Te atoms and vacancy are denoted in purple, red, pink, and white, respectively). (b) Rietveld refinement of the room-temperature powder X-ray diffraction pattern for LuCuTe$_2$. The experimental data are shown as a black curve; the simulated pattern from the LuCuTe$_2$ and LuTe$_2$ two-phase structural model is plotted in red, and the difference curve is denoted in a green offset below. The ticks indicate the calculated reflection positions of phases. (c) SEM image and corresponding EDS mapping for the obtained LuCuTe$_2$. (d) X-ray PDF of room-temperature data fit by the LuCuTe$_2$ and LuTe$_2$ two-phase structural model. The fit range was set to 2 to 9.5 Å. The experiment data, structural model, and difference curve are shown in blue, red, and green, respectively. The fit quality is $R_w = 0.2739$.

Table 1. Theoretical and Practical Interatomic Distances and Coordination Numbers (C.N.) of the Lu and Cu Atoms in LuCuTe$_2$

atoms	theoretical distance (Å)	practical distance (Å)	C.N.
Lu1−Te	3.026(1)	3.0552	6
Lu2−Te	2.983(1)	2.9927	
Cu1−Te	2.585(5)/2.582(1)	2.5747/2.6600	4
Cu2−Te	2.42(5)/2.70(2)	2.3817/2.7487	
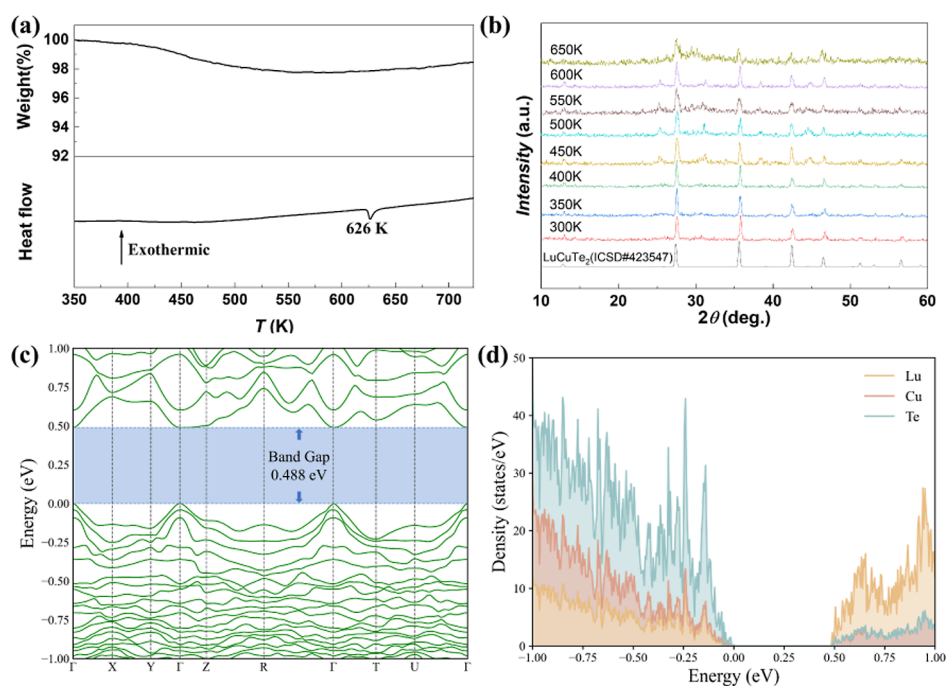
Figure 2. Weight and heat flow (b) as a function of temperature (a), powder XRD patterns at different temperatures (b), calculated band structure (c), and projected density of states of each element (d) for pristine $LuCuTe_2$. The valence band maximum is set to 0 eV.
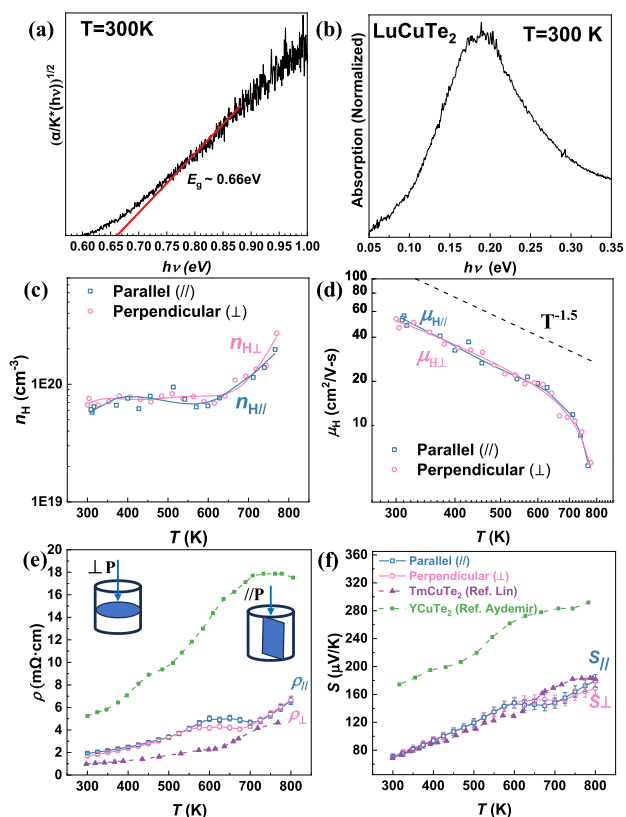

Figure 3. Normalized optical absorption versus photon energy between band edges (a) and free carriers (b) for $LuCuTe_2$. Temperature-dependent Hall carrier concentration (c), Hall mobility (d), resistivity (e), and Seebeck coefficient (f) for $LuCuTe_2$ pellets sliced perpendicular to the hot-pressed direction ($\perp$) and parallel to the hot-pressed direction ($//$), with a comparison to those of previously reported $ReCuTe_2$.[31,56]

B—A formed by copper and telluride atoms, with Lu^{3+} located in the layers, with a probability of 76.5 and 23.5% Lu occupations at 1a and 1b sites, respectively, and 31 and 19% Cu occupations at 2d sites (Figure 1a). The Lu and Cu atoms are distributed over the octahedral and tetrahedral positions, respectively. The intrinsically high Cu and Lu atom site disordering would strengthen the anharmonicity for strong phonon scattering.

The room-temperature powder XRD data of the synthesized sample are depicted in Figure 1b. Most of the diffraction Bragg peaks can be matched to the $P\bar{3}m1LuCuTe_2$ phase reasonably well, which can be further validated by SEM observation and EDS analysis (Figure 1c). According to the Rietveld refinement obtained by GSAS II software (Figure 1b), a small amount of the $LuTe_2$ impurity phase is found in the sample, and the atomic percentage of the impurity phase $LuTe_2$ is refined to be about 2.5%. The presence of precipitates would cause additional scattering on the hole carriers and phonons, resulting in decreased carrier mobility and lattice thermal conductivity. From the refinement results, there is a slight mismatch in the peak intensities between the crystallographic structure and diffraction data, and this may indicate a possible cation disordering in the material.

To further investigate the local atomic disordering, the synchrotron X-ray PDF local structure analysis is carried out, which can reveal the interatomic distances between atom sites beyond the long-range average structure, as shown in Figure 1d and Figure S1. A $LuCuTe_2$ structure model with a small amount of $LuTe_2$ impurity fits well with the experiment data. Table 1 and Table S1 list the short-range structure information extracted from the experimental PDF, which aligns well with results reported in the existing literature,[33,51] further confirming the structural stability of the synthesized material.

Based on the TG analysis (Figure 2a), $LuCuTe_2$ shows a mass loss of ~2% as the temperature increases to 500 K, which probably stems from the evaporation of moisture. The nearly
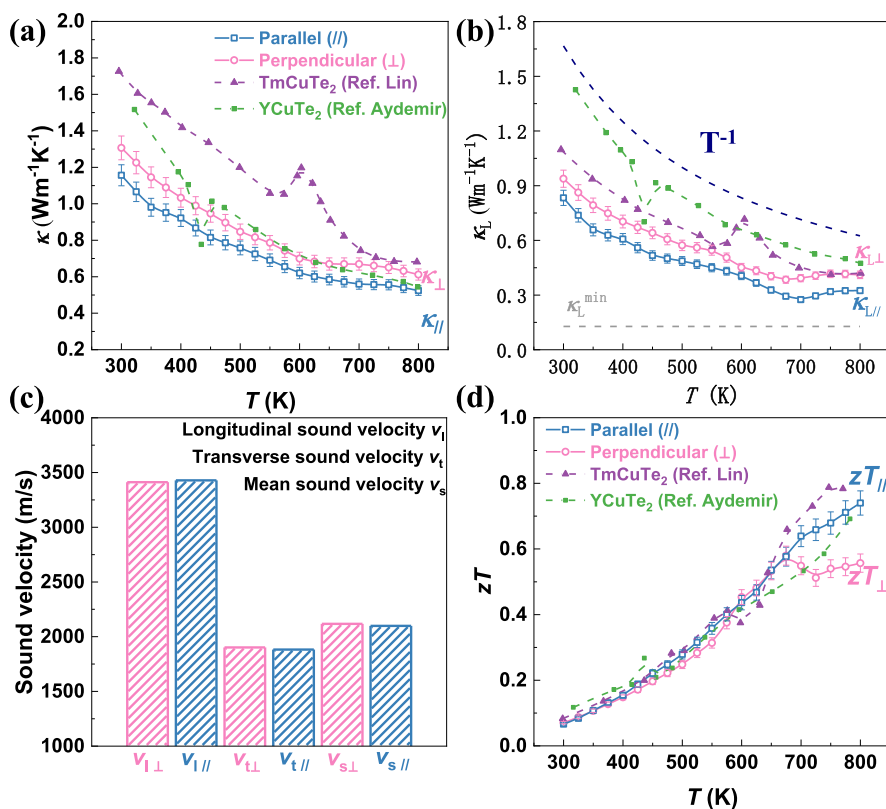
Figure 4. Thermal conductivities, sound velocities (c), and temperature-dependent zT (d) for LuCuTe$_2$, with a comparison to those of previously reported ReCuTe$_2$.[31,56]
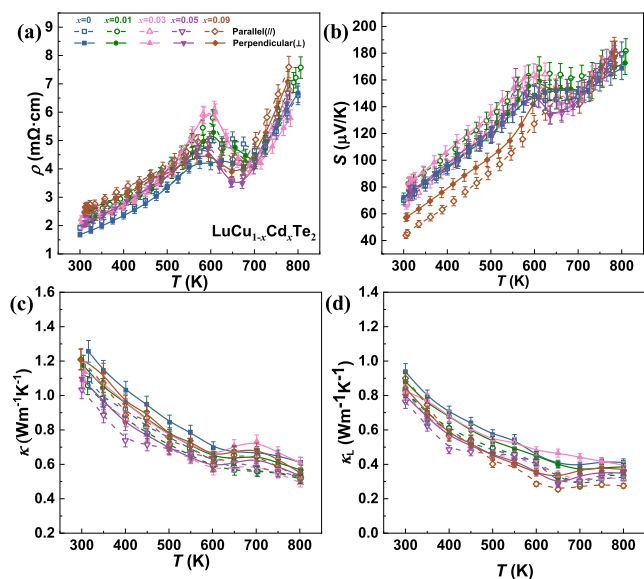
Figure 5. Temperature-dependent resistivity (a), Seebeck coefficient (b), total (c), and lattice (d) thermal conductivity for LuCu$_{1-x}$Cd$_x$Te$_2$.

constant mass at temperatures higher than 500 K confirms its thermal stability. A phase transition occurs at ~626 K according to the DSC result (Figure 2b), which is further confirmed by the high-temperature XRD results (Figure 2b). A similar case has also been observed in TmCuTe$_2$.[27,51]

The calculated band structure and projected density of states for pristine LuCuTe$_2$ are shown in Figure 2c,d, respectively. The conduction band minimum and valence band maximum

are located at the Γ position of the Brillouin zone, with contributions from Lu and Cu atoms, respectively. The theoretical direct band gap (E_g) is approximately ~0.46 eV, which is smaller than the E_g (~0.66 eV) estimated from optical measurement[52] (Figure 3a). Such a difference can be possibly attributed to the underestimation of E_g using the PBE exchange−correlation functional.[53]

Furthermore, the inertial effective mass (m_I^*) could be obtained according to free carrier absorption versus photon energy (Figure 3b) through the Lyden method, given by $m_I^* = ne^2/\omega_0^2\varepsilon_0\varepsilon_\infty$,[54] where ω_0 is the angular frequency of the absorption maximum, e is the electronic charge, n is the carrier concentration, ε_0 represents the permittivity of free space, and ε_∞ (~14 for LuCuTe$_2$) refers to the high-frequency dielectric constant estimated by the Ravindra method.[55] As a result, m_I^* for LuCuTe$_2$ is estimated to be ~0.21 m_e.

Note that the trigonal crystal structure would possibly enable an anisotropy in transport properties, and the thermoelectric transport properties of two pellets sliced perpendicular to the hot-pressed direction ($\perp$) and parallel to the hot-pressed direction ($//$) were studied. Temperature-dependent electrical transport properties are shown in Figure 3c−f. Pristine LuCuTe$_2$ shows a Hall carrier concentration (n_H) of ~6 × 10^{19} cm^{-3} (Figure 3c) together with a Hall mobility (μ_H) of ~60 cm^2/V s (Figure 3d). The increases in n_H at a temperature higher than 600 K are presumably attributed to the phase transition.[56] Temperature-dependent μ_H follows the relationship of $\mu_H \sim T^{-1.5}$, illustrating the dominant mechanism of charge carrier scattering by acoustic phonons. The positive Seebeck coefficient represents p-type conduction. Both resistivity and Seebeck coefficient increase with increasing temperature, while the anomaly between 600 and

Table 2. Measured Sound Velocity and the Estimated Physical Parameters [Grueneisen Parameter γ, Poisson's Ratio ε, Debye Temperature θ_D, Shear Modulus G, and Bulk Modulus B for LuCu$_{1-x}$Cd$_x$Te$_2$ ($0 \leq x \leq 0.9$)]

materials	v_l (m/s)	v_t (m/s)	θ_D (K)	ε	G (GPa)	B (GPa)	γ
$x = 0.00$	3430	1880	132	0.28	25.9	51.3	1.68
$x = 0.01$	3114	1734	122	0.28	21.5	40.7	1.63
$x = 0.03$	3200	1720	121	0.30	21.2	45.2	1.76
$x = 0.05$	3290	1810	127	0.28	23.6	46.5	1.67
$x = 0.09$	3470	1880	132	0.29	25.2	52.9	1.74
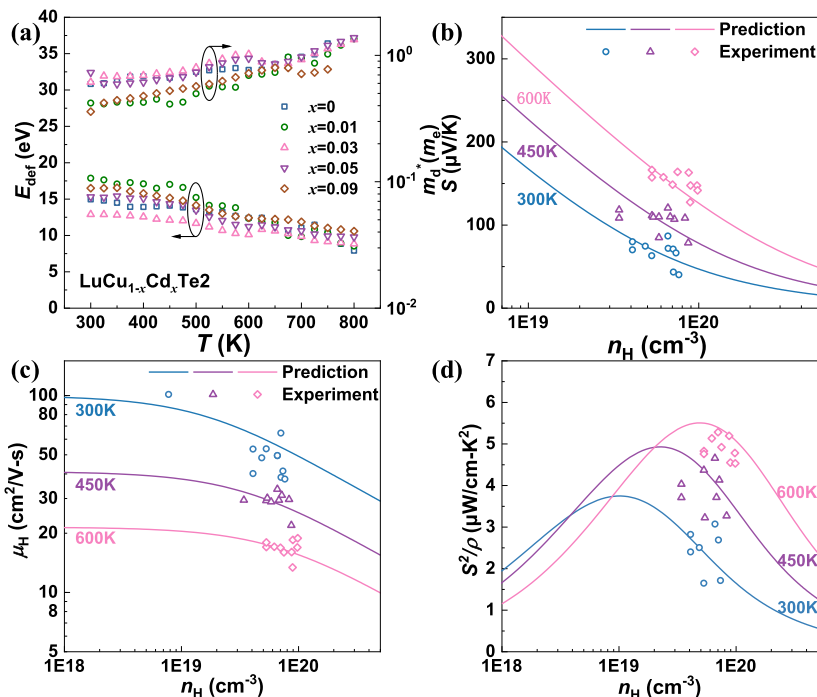
Figure 6. Temperature-dependent deformation potential coefficient (E_{def}) and density-of-state effective mass (m_d*) (a), Hall carrier concentration (n_H)-dependent Seebeck coefficient (b), Hall mobility (c), and power factor (S^2/ρ) (d) at various temperatures for LuCu$_{1-x}$Cd$_x$Te$_2$.
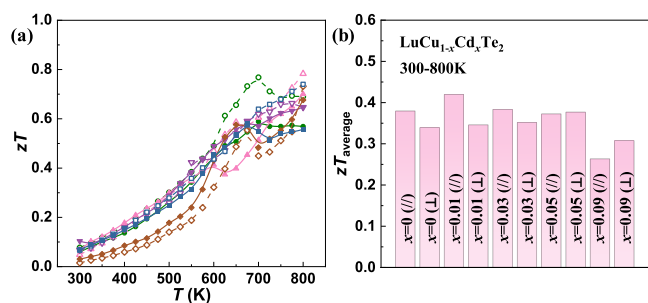
Figure 7. Temperature-dependent zT (a) and the average zT within a temperature range of 300−800 K (b) for LuCu$_{1-x}$Cd$_x$Te$_2$.

700 K presumably originates from a structural phase transition. A similar condition has also been observed in GeTe-based thermoelectrics[57] and other ReCuTe$_2$.[31,34,56] The comparable transport properties for the pellets along different directions suggest isotropic electrical transport properties.

The total (κ) and lattice (κ_L) thermal conductivity along different directions are shown in Figure 4a,b, respectively. The electronic thermal conductivity (κ_E) can be calculated according to the Wiedemann−Franz law, $\kappa_E = LT/\rho$, where L represents the Lorenz number determined by a SPB model.[58] The κ_L is estimated by subtracting κ_E from κ. At room temperature, κ_L along the directions normal and parallel to that

of hot-pressed one are determined as 0.94 and 0.88 W/m K, respectively, the difference of which can be understood by the measurement deviations, illustrating the isotropic thermal transport properties. Moreover, both κ_L decrease with rising temperature following the $\kappa_L \sim T^{-1}$ relationship, indicating that the phonon scattering is dominated by the Umklapp process.

The longitudinal (v_l) and transverse (v_t) sound velocities are obtained and are depicted in Figure 4c. Both are found to be comparable to those of the IV−VI group thermoelectrics.[59−61] Therefore, the low κ_L in LuCuTe$_2$ stems from the strong phonon scattering because of the substantial atomic disorder. Consequently, a peak figure of merit, zT, of ~0.8, is realized at 800 K for LuCuTe$_2$ (Figure 4d). The amorphous limit (κ_L^{min}) is estimated by the model considering the influence of Born-von Karman periodic boundary conditions[62] (gray dashed line in Figure 4b), which is much lower than the experimental κ_L in the entire temperature range. This suggests that there is room to further reduce κ_L through microstructure engineering for the enhanced zT.

Cd-substitution at the Cu site is applied for manipulating the n_H for evaluating transport properties. Powder XRD patterns for LuCu$_{1-x}$Cd$_x$Te$_2$, shown in Figure S2, reveal an appearance of CdTe precipitates in addition to LuCuTe$_2$. This elucidates the low doping solubility of Cd, which can be further identified by the nearly unchanged lattice parameters (Figure S3 and

Table S2) and slightly changed n_H ($4-6 \times 10^{19}$ cm^{-3}, Figure S4a) for LuCu$_{1-x}$Cd$_x$Te$_2$. The solubility is estimated to be lower than 0.5% according to the EDS results of LuCu$_{0.99}$Cd$_{0.01}$Te$_2$, stemming from the resolution limit of 0.5% for the facility (Figure S5). Cd-doping does not change the mechanism of the charge carrier scattering (Figure S4b). The optical E_g for the doped samples is estimated to be 0.66 eV (Figure S6), and it remains independent of the composition.

The transport properties for the doped samples, measured along the directions perpendicular and parallel to the hot-pressed one, are shown in Figure 5. The slight difference in the electrical transport properties comes from the contribution of slightly changed n_H. The consistent results of transport properties for pristine LuCuTe$_2$ measured during heating and cooling reveal the reproducibility and thermal stability (Figure S7). As $x \leq 0.05$, the κ_L decreases with increasing x because of the extra phonon scattering from Cd/Cu substitutional point defects and CdTe precipitates, while it increases as $x > 0.05$ due to the increased concentration of CdTe with a high κ_L.[63] The similarities in sound velocities for the doped samples exclude the contribution of the sound velocity to κ_L-reduction (Table 2). Furthermore, their physical parameters of Gruneisen parameter γ, Poisson's ratio ε, Debye temperature (θ_D), shear modulus G, and bulk modulus B are estimated using the measured sound velocities.[64]

Based on the results of Hall measurement, a SPB model incorporating acoustic scattering is employed to illustrate the underlying material's parameters and predict the electrical transport properties. In doped LuCuTe$_2$, an average density-of-state effective mass (m_d^*) of ~0.5 m_e and an average deformation potential coefficient (E_{def}) of ~15 eV (Figure 6a) are obtained. Both parameters show nearly independent behavior with the dopants, suggesting a rigid band behavior. Utilizing the estimated m_d^* and E_{def}, the n_H-dependent Seebeck coefficient, Hall mobility, and power factor can be predicted reasonably by the SPB model at various temperatures, as depicted in Figure 6b−d.

Moreover, temperature-dependent zT and average zT within the measured temperature are, respectively, shown in Figure 7a,b. Stemming from the further reduction in κ_L, a peak zT of 0.8 and the average zT of ~0.4 are achieved in LuCu$_{0.99}$Cd$_{0.01}$Te$_2$. The results clearly suggest this material is a promising option for thermoelectric applications.

4. SUMMARY

In summary, p-type LuCuTe$_2$ with an E_g of 0.66 eV exhibits isotropic transport properties. Due to the existence of the substantial atomic disorder for strong phonon scattering, the lattice thermal conductivity is lower than 1.0 W/m-K over the temperature range of 300−800 K, and the lowest value of 0.3 W/m-K is achieved. A peak zT of ~0.8 is realized in the LuCuTe$_2$-based thermoelectric. This work suggests that this material may serve as a promising thermoelectric candidate and provides the routes for enhancing zT through further reduction in lattice thermal conductivity by microstructure engineering.

ASSOCIATED CONTENT

ⓈⒾ Supporting Information

The Supporting Information is available free of charge at https://pubs.acs.org/doi/10.1021/acsaem.4c00763.

X-ray PDF data processing, analysis, and refinement results of LuCuTe$_2$; Rietveld refinement plots and refined lattice parameters for LuCu$_{1-x}$Cd$_x$Te$_2$; normalized absorption versus photon energy for Lu-Cu$_{1-x}$Cd$_x$Te$_2$; SEM image and EDS results for LuCu$_{0.97}$Cd$_{0.03}$Te$_2$; transport properties for pristine LuCuTe$_2$ measured during heating and cooling; and equations of the model involving the effect of Born-von Karman periodic boundary conditions (PDF)

■ AUTHOR INFORMATION

Corresponding Authors

Long Yang − *Interdisciplinary Materials Research Center, School of Materials Science and Engineering, Tongji Univ., Shanghai 201804, China*; Email: long_yang@tongji.edu.cn

Wen Li − *Interdisciplinary Materials Research Center, School of Materials Science and Engineering, Tongji Univ., Shanghai 201804, China*; ⓞ orcid.org/0000-0001-8912-3792; Email: liwen@tongji.edu.cn

Authors

Xiaoyu Zhang − *Interdisciplinary Materials Research Center, School of Materials Science and Engineering, Tongji Univ., Shanghai 201804, China*

Changyuan Li − *Interdisciplinary Materials Research Center, School of Materials Science and Engineering, Tongji Univ., Shanghai 201804, China*

Yuting Meng − *Interdisciplinary Materials Research Center, School of Materials Science and Engineering, Tongji Univ., Shanghai 201804, China*

Complete contact information is available at:
https://pubs.acs.org/10.1021/acsaem.4c00763

Author Contributions

†X.Z and C.L. equally contributed.

Notes

The authors declare no competing financial interest.

■ ACKNOWLEDGMENTS

■ REFERENCES

(1) Pei, Y.; Shi, X.; LaLonde, A.; Wang, H.; Chen, L.; Snyder, G. J. Convergence of Electronic Bands for High Performance Bulk Thermoelectrics. *Nature* **2011**, *473* (7345), 66−69.

(2) Pei, Y.; LaLonde, A. D.; Wang, H.; Snyder, G. J. Low Effective Mass Leading to High Thermoelectric Performance. *Energy Environ. Sci.* **2012**, *5* (7), 7963−7969.

(3) Wang, H.; Pei, Y.; LaLonde, A. D.; Snyder, G. J. Weak Electron-phonon Coupling Contributing to High Thermoelectric Performance in n-type PbSe. *Proc. Natl. Acad. Sci. U.S.A.* **2012**, *109* (25), 9705−9709.

(4) Pei, Y.; Wang, H.; Snyder, G. J. Band Engineering of Thermoelectric Materials. *Adv. Mater.* **2012**, *24* (46), 6125−6135.

(5) Liu, W.; Tan, X. J.; Yin, K.; Liu, H. J.; Tang, X. F.; Shi, J.; Zhang, Q. J.; Uher, C. Convergence of Conduction Bands as a Means of

Enhancing Thermoelectric Performance of n-Type $Mg_2Si_{1-x}Sn_x$ Solid Solutions. *Appl. Phys. Lett.* 2012, 108 (16), 166601.

(6) Li, J.; Zhang, X.; Chen, Z.; Lin, S.; Li, W.; Shen, J.; Witting, I. T.; Faghaninia, A.; Chen, Y.; Jain, A.; Chen, L.; Snyder, G. J.; Pei, Y. Low-Symmetry Rhombohedral GeTe Thermoelectrics. *Joule* 2018, 2 (5), 976−987.

(7) Zhang, X.; Li, J.; Wang, X.; Chen, Z.; Mao, J.; Chen, Y.; Pei, Y. Vacancy Manipulation for Thermoelectric Enhancements in GeTe Alloys. *J. Am. Chem. Soc.* 2018, 140 (46), 15883−15888.

(8) Zhao, L. D.; Wu, H. J.; Hao, S. Q.; Wu, C. I.; Zhou, X. Y.; Biswas, K.; He, J. Q.; Hogan, T. P.; Uher, C.; Wolverton, C.; Dravid, V. P.; Kanatzidis, M. G. All-scale Hierarchical Thermoelectrics: MgTe in PbTe Facilitates Valence Band Convergence and Suppresses Bipolar Thermal Transport for High Performance. *Energy Environ. Sci.* 2013, 6 (11), 3346−3355.

(9) Li, W.; Zheng, L.; Ge, B.; Lin, S.; Zhang, X.; Chen, Z.; Chang, Y.; Pei, Y. Promoting SnTe as an Eco-Friendly Solution for p-PbTe Thermoelectric via Band Convergence and Interstitial Defects. *Adv. Mater.* 2017, 29 (17), 1605887.

(10) Chen, Z.; Jian, Z.; Li, W.; Chang, Y.; Ge, B.; Hanus, R.; Yang, J.; Chen, Y.; Huang, M.; Snyder, G. J.; Pei, Y. Lattice Dislocations Enhancing Thermoelectric PbTe in Addition to Band Convergence. *Adv. Mater.* 2017, 29 (23), 1606768.

(11) Zhang, J.; Song, L.; Pedersen, S. H.; Yin, H.; Hung, L. T.; Iversen, B. B. Discovery of High-performance Low-cost n-type Mg3Sb2-based Thermoelectric Materials with Multi-valley Conduction Bands. *Nat. Commun.* 2017, 8, 13901.

(12) Liu, Y.; Fu, C.; Xia, K.; Yu, J.; Zhao, X.; Pan, H.; Felser, C.; Zhu, T. Lanthanide Contraction as a Design Factor for High-Performance Half-Heusler Thermoelectric Materials. *Adv. Mater.* 2018, 30 (32), 1800881.

(13) Fu, C. G.; Zhu, T. J.; Pei, Y. Z.; Xie, H. H.; Wang, H.; Snyder, G. J.; Liu, Y.; Liu, Y. T.; Zhao, X. B. High Band Degeneracy Contributes to High Thermoelectric Performance in p-Type Half-Heusler Compounds. *Adv. Energy Mater.* 2014, 4 (18), 1400600.

(14) Lin, S. Q.; Li, W.; Chen, Z. W.; Shen, J. W.; Ge, B. H.; Pei, Y. Z. Tellurium as a High-performance Elemental Thermoelectric. *Nat. Commun.* 2016, 7 (1), 10287.

(15) Tang, Y.; Gibbs, Z. M.; Agapito, L. A.; Li, G.; Kim, H.-S.; Nardelli, M. B.; Curtarolo, S.; Snyder, J. Convergence of Multi-valley Bands as the Electronic Origin of High Thermoelectric Performance in CoSb₃ Skutterudites. *Nat. Mater.* 2015, 14, 1223−1228.

(16) Zheng, L.; Li, W.; Wang, X.; Pei, Y. Alloying for Orbital Alignment Enables Thermoelectric Enhancement of EuCd2Sb2. *J. Mater. Chem. A* 2019, 7 (20), 12773−12778.

(17) Zhang, J.; Song, L.; Madsen, G. K.; Fischer, K. F.; Zhang, W.; Shi, X.; Iversen, B. B. Designing High-performance Layered Thermoelectric Materials Through Orbital Engineering. *Nat. Commun.* 2016, 7, 10892.

(18) Li, S. H.; Hinckley, J. M.; Singh, J.; Bhattacharya, P. K. Carrier velocity-field characteristics and alloy scattering potential in Si1−xGex/Si. *Appl. Phys. Lett.* 1993, 63 (10), 1393−1395.

(19) Kim, S. I.; Lee, K. H.; Mun, H. A.; Kim, H. S.; Hwang, S. W.; Roh, J. W.; Yang, D. J.; Shin, W. H.; Li, X. S.; Lee, Y. H.; et al. Dense Dislocation Arrays Embedded in Grain Boundaries for High-performance Bulk Thermoelectrics. *Science* 2015, 348 (6230), 109−114.

(20) Xin, J.; Wu, H.; Liu, X.; Zhu, T.; Yu, G.; Zhao, X. Mg Vacancy and Dislocation Strains as Strong Phonon Scatterers in $Mg_2Si_{1-x}Sb_x$ Thermoelectric Materials. *Nano Energy* 2017, 34, 428−436.

(21) Qin, C.; Cheng, L.; Xiao, Y.; Wen, C.; Ge, B.; Li, W.; Pei, Y. Substitutions and Dislocations Enabled Extraordinary n-type Thermoelectric PbTe. *Mater. Today Phys.* 2021, 17, 100355.

(22) Biswas, K.; He, J.; Blum, I. D.; Wu, C.-I.; Hogan, T. P.; Seidman, D. N.; Dravid, V. P.; Kanatzidis, M. G. High-Performance Bulk Thermoelectrics with All-scale Hierarchical Architectures. *Nature* 2012, 489 (7416), 414−418.

(23) Hsu, K. F.; Loo, S.; Guo, F.; Chen, W.; Dyck, J. S.; Uher, C.; Hogan, T.; Polychroniadis, E. K.; Kanatzidis, M. G. Cubic

$AgPb_mSbTe_{2+m}$: Bulk Thermoelectric Materials with High Figure of Merit. *Science* 2004, 303 (5659), 818−821.

(24) Lin, S.; Li, W.; Li, S.; Zhang, X.; Chen, Z.; Xu, Y.; Chen, Y.; Pei, Y. High Thermoelectric Performance of Ag₉GaSe₆ Enabled by Low Cutoff Frequency of Acoustic Phonons. *Joule* 2017, 1, 816−830.

(25) Liu, H.; Yuan, X.; Lu, P.; Shi, X.; Xu, F.; He, Y.; Tang, Y.; Bai, S.; Zhang, W.; Chen, L.; Lin, Y.; Shi, L.; Lin, H.; Gao, X.; Zhang, X.; Chi, H.; Uher, C. Ultrahigh Thermoelectric Performance by Electron and Phonon Critical Scattering in $Cu_2Se_{1-x}I_x$. *Adv. Mater.* 2013, 25 (45), 6607−6612.

(26) Li, W.; Lin, S.; Weiss, M.; Chen, Z.; Li, J.; Xu, Y.; Zeier, W. G.; Pei, Y. Crystal Structure Induced Ultralow Lattice Thermal Conductivity in Thermoelectric Ag9AlSe6. *Adv. Energy Mater.* 2018, 8 (18), 1800030.

(27) Bai, Q.; Zhang, X.; Shan, B.; Shi, X.; Sun, C.; Lin, S.; Li, W.; Pei, Y. Thermoelectric Transport Properties of $TmAg_xCu_{1-x}Te_2$ solid solutions. *J. Materiomics* 2021, 7 (4), 886−893.

(28) Zhang, D.; Zhang, B.; Zhou, Z.; Peng, K.; Wu, H.; Wang, H.; Wang, G.; Han, G.; Wang, G.; Zhou, X.; Lu, X. Ultralow Lattice Thermal Conductivity of Cubic CuFeS₂ Induced by Atomic Disorder. *Chem. Mater.* 2021, 33 (24), 9795−9802.

(29) Li, C. W.; Hong, J.; May, A. F.; Bansal, D.; Chi, S.; Hong, T.; Ehlers, G.; Delaire, O. Orbitally Driven Giant Phonon Anharmonicity in SnSe. *Nat. Phys.* 2015, 11 (12), 1063−1069.

(30) Tang, J.; Qin, C.; Yu, H.; Zeng, Z.; Cheng, L.; Ge, B.; Chen, Y.; Li, W.; Pei, Y. Ultralow Lattice Thermal Conductivity Enables High Thermoelectric Performance in BaAg₂Te₂ Alloys. *Mater. Today Phys.* 2022, 22, 100591.

(31) Lin, H.; Chen, H.; Ma, N.; Zheng, Y.-J.; Shen, J.-N.; Yu, J.-S.; Wu, X.-T.; Wu, L.-M. Syntheses, Structures, and Thermoelectric Properties of Ternary Tellurides: RECuTe2 (RE = Tb-Er). *Inorg. Chem. Front.* 2017, 4 (8), 1273−1280.

(32) Esmaeili, M.; Forbes, S.; Tseng, Y.-C.; Mozharivskyj, Y. Crystal Structure, Electronic and Physical Properties of Monoclinic RECuTe₂ in Contrast to RECuSe₂ (RE = Pr, Sm, Gd, Dy and Er). *Solid State Sci.* 2014, 36, 89−93.

(33) Gulay, L. D.; Daszkiewicz, M.; Shemet, V. Y. Crystal Structure of ∼ RCu₃S₃ and ∼ RCuTe₂ (R = Gd-Lu) Compounds. *J. Solid State Chem.* 2012, 186, 142−148.

(34) Lin, H.; Chen, H.; Shen, J. N.; Chen, L.; Wu, L. M. Chemical Modification and Energetically Favorable Atomic Disorder of a Layered Thermoelectric Material TmCuTe2 Leading to High Performance. *Chemistry* 2014, 20 (47), 15401−15408.

(35) Dong, J.; Jiang, Y.; Sun, Y.; Liu, J.; Pei, J.; Li, W.; Tan, X. Y.; Hu, L.; Jia, N.; Xu, B.; Li, Q.; Li, J.-F.; Yan, Q.; Kanatzidis, M. G. Discordant Distortion in Cubic GeMnTe2 and High Thermoelectric Properties of GeMnTe2-x%SbTe. *J. Am. Chem. Soc.* 2023, 145 (3), 1988−1996.

(36) Takeshi, E.; Billinge, S. J. L. Chapter 3—The Method of Total Scattering and Atomic Pair Distribution Function Analysis. In *Pergamon Materials Series*; Egami, T., Billinge, S. J. L., Eds.; Pergamon, 2012; pp 55−111.

(37) Chupas, P. J.; Qiu, X.; Hanson, J. C.; Lee, P. L.; Grey, C. P.; Billinge, S. J. L. Rapid-acquisition Pair Distribution Function (RA-PDF) Analysis. *J. Appl. Crystallogr.* 2003, 36 (6), 1342−1347.

(38) Proffen, T.; Billinge, S. J. L. PDFFIT, A Program for Full Profile Structural Refinement of the Atomic Pair Distribution Function. *J. Appl. Crystallogr.* 1999, 32 (3), 572−575.

(39) Farrow, C. L.; Juhas, P.; Liu, J. W.; Bryndin, D.; Božin, E. S.; Bloch, J.; Proffen, T.; Billinge, S. J. L. PDFfit2 and PDFgui: Computer Programs for Studying Nanostructure in Crystals. *J. Phys.: Condens. Matter* 2007, 19 (33), 335219.

(40) Kieffer, J.; Karkoulis, D. PyFAI, A Versatile Library for Azimuthal Regrouping. *J. Phys.: Conf. Ser.* 2013, 425 (20), 202012.

(41) Juhas, P.; Davis, T.; Farrow, C. L.; Billinge, S. J. L. PDFgetX3: a Rapid and Highly Automatable Program for Processing Powder Diffraction Data Into Total Scattering Pair Distribution Functions. *J. Appl. Crystallogr.* 2013, 46 (2), 560−566.

G

(42) Zunger, A.; Wei, S. H.; Ferreira, L. G.; Bernard, J. E. Special Quasirandom Structures. *Phys. Rev. Lett.* **1990**, *65* (3), 353−356.

(43) Zhang, J.; Su, C.; Liu, Y. First-principles study of bcc Fe-Cr-Si Binary and Ternary Random Alloys from Special Quasi-random Structure. *Phys. B* **2020**, *586*, 412085.

(44) van de Walle, A.; Asta, M.; Ceder, G. The Alloy Theoretic Automated Toolkit: A user guide. *Calphad* **2002**, *26* (4), 539−553.

(45) Jiang, B.; Bridges, C. A.; Unocic, R. R.; Pitike, K. C.; Cooper, V. R.; Zhang, Y.; Lin, D.-Y.; Page, K. Probing the Local Site Disorder and Distortion in Pyrochlore High-Entropy Oxides. *J. Am. Chem. Soc.* **2021**, *143* (11), 4193−4204.

(46) Luo, Y.; Xu, T.; Ma, Z.; Zhang, D.; Guo, Z.; Jiang, Q.; Yang, J.; Yan, Q.; Kanatzidis, M. G. Cubic AgMnSbTe3 Semiconductor with a High Thermoelectric Performance. *J. Am. Chem. Soc.* **2021**, *143* (34), 13990−13998.

(47) Dahlqvist, M.; Tao, Q.; Zhou, J.; Palisaitis, J.; Persson, P. O. Å.; Rosen, J. Theoretical Prediction and Synthesis of a Family of Atomic Laminate Metal Borides with In-Plane Chemical Ordering. *J. Am. Chem. Soc.* **2020**, *142* (43), 18583−18591.

(48) Kresse, G.; Furthmüller, J. Efficiency of Ab-initio Total Energy Calculations for Metals and Semiconductors Using a Plane-wave Basis Set. *Comput. Mater. Sci.* **1996**, *6* (1), 15−50.

(49) Kresse, G.; Joubert, D. From Ultrasoft Pseudopotentials to the Projector Augmented-wave Method. *Phys. Rev. B* **1999**, *59* (3), 1758−1775.

(50) Perdew, J. P.; Burke, K.; Ernzerhof, M. Generalized Gradient Approximation Made Simple. *Phys. Rev. Lett.* **1996**, *77* (18), 3865−3868.

(51) Lin, H.; Chen, H.; Shen, J. N.; Chen, L.; Wu, L. M. Chemical Modification and Energetically Favorable Atomic Disorder of a Layered Thermoelectric Material TmCuTe$_2$ Leading to High Performance. *Chem.—Eur. J.* **2014**, *20* (47), 15401−15408.

(52) Gibbs, Z. M.; LaLonde, A.; Snyder, G. J. Optical Band Gap and the Burstein-Moss Effect in Iodine Doped PbTe Using Diffuse Reflectance Infrared Fourier Transform Spectroscopy. *New J. Phys.* **2013**, *15* (7), 075020.

(53) Kümmel, S.; Kronik, L. Orbital-dependent Density Functionals: Theory and Applications. *Rev. Mod. Phys.* **2008**, *80* (1), 3−60.

(54) Lyden, H. A. Measurement of the Conductivity Effective Mass in Semiconductors Using Infrared Reflection. *Phys. Rev.* **1964**, *134* (4A), A1106−A1112.

(55) Moss, T. S. Relations Between the Refractive Index and Energy Gap of Semiconductors. *Phys. Status Solidi B* **1985**, *131* (2), 415−427.

(56) Aydemir, U.; Pöhls, J. H.; Zhu, H.; Hautier, G.; Bajaj, S.; Gibbs, Z. M.; Chen, W.; Li, G.; Ohno, S.; Broberg, D.; Kang, S. D.; Asta, M.; Ceder, G.; White, M. A.; Persson, K.; Jain, A.; Snyder, G. J. YCuTe2: A Member of a New Class of Thermoelectric Materials with CuTe4-based Layered Structure. *J. Mater. Chem. A* **2016**, *4* (7), 2461−2472.

(57) Li, J.; Zhang, X.; Lin, S.; Chen, Z.; Pei, Y. Realizing the High Thermoelectric Performance of GeTe by Sb-doping and Se-alloying. *Chem. Mater.* **2017**, *29* (2), 605−611.

(58) May, A. F.; Toberer, E. S.; Saramat, A.; Snyder, G. J. Characterization and analysis of thermoelectric transport in n-type Ba$_8$Ga$_{16-x}$Ge$_{30+x}$. *Phys. Rev. B* **2009**, *80* (12), 125205.

(59) Li, J.; Chen, Z.; Zhang, X.; Yu, H.; Wu, Z.; Xie, H.; Chen, Y.; Pei, Y. Simultaneous Optimization of Carrier Concentration and Alloy Scattering for Ultrahigh Performance GeTe Thermoelectrics. *Adv. Sci.* **2017**, *4* (12), 1700341.

(60) Li, W.; Chen, Z.; Lin, S.; Chang, Y.; Ge, B.; Chen, Y.; Pei, Y. Band and Scattering Tuning for High Performance Thermoelectric Sn1- xMnxTe alloys. *J. Materiomics* **2015**, *1* (4), 307−315.

(61) Wang, H.; Schechtel, E.; Pei, Y.; Snyder, G. J. High Thermoelectric Efficiency of n-type PbS. *Adv. Energy Mater.* **2013**, *3* (4), 488−495.

(62) Chen, Z.; Zhang, X.; Lin, S.; Chen, L.; Pei, Y. Rationalizing Phonon Dispersion for Lattice Thermal Conductivity of Solids. *Natl. Sci. Rev.* **2018**, *5* (6), 888−894.

(63) Su, C.-H. Thermal Conductivity, Electrical Conductivity, and Thermoelectric Properties of CdTe and Cd$_{0.8}$Zn$_{0.2}$Te Crystals Between Room Temperature and 780 °C. *AIP Adv.* **2015**, *5* (5), 057118.

(64) Roufosse, M.; Klemens, P. G. Thermal Conductivity of Complex Dielectric Crystals. *Phys. Rev. B* **1973**, *7* (12), 5379−5386.